Polymer Degradation and Stability 189 (2021) 109599

Contents lists available at ScienceDirect

Polymer Degradation and Stability

journal homepage: www.elsevier.com/locate/polymdegradstab

An addition-curable hybrid phenolic resin containing silicon and boron with improved thermal stability

Youpei Du[a,b], Yu Xia[c], Zhenhua Luo[a,*], Wenjie Yuan[a,b], Kongli Xu[c], Qian Wang[a], Heng Zhou[a], Ying Guo[a], Hao Li[a], Tong Zhao[a,b,*]

[a] Key Laboratory of Science and Technology on High-tech Polymer Materials, Institute of Chemistry, Chinese Academy of Sciences
[b] University of Chinese Academy of Sciences, Beijing 100049, China
[c] Research Institute of Aerospace Special Materials and Process Technology, Beijing 100049, China

ARTICLE INFO

Article history:
Received 11 February 2021
Revised 10 April 2021
Accepted 21 April 2021
Available online 24 April 2021

Keywords:
Phenolic resin
Synergistic hybrid
Addition cure
Thermal stability

ABSTRACT

In this work, an addition-curable hybrid phenolic resin containing silicon and boron was synthesized via the addition-condensation reaction between 4-hydroxyphenylboronic acid and formaldehyde to obtain boron hybrid novolac resin (BN), which was followed by esterification with vinyltrimethoxysilane. Boron and silicon were introduced into the phenolic resin skeleton by forming C-B-OH, B-O-C, B-O-Si, and Si-O-Ph bonds, so the hybrid resin not only realized uniform molecular-level dispersion of hybrid elements but also achieved addition curing via the presence of vinyl groups. The hybrid resin's residual weight in an N_2 atmosphere at 800°C was improved to 81.02%. The high residual weight arose from the formation of a three-dimensional continuous oxide framework composed of B-O-B-O-Si-O-Si. In addition, we characterized the pyrosis production of the materials with the combination of FT-IR, Raman, SEM/SEM-EDX, XPS, and solid-state NMR spectroscopy to develop a detailed understanding of the synergistic effects of boron-silicon modified phenolic resin.

1. Introduction

Phenolic resin (PR), as an irreplaceable member of the thermoset family, has been widely used in thermal insulation, coatings, adhesives and ablative materials owing to its excellent properties, such as thermal stability, high char yield, high hardness, and flame retardancy. However, with the growth of the aerospace industry, the application of PR has been impeded by some of its inherent qualities, including the formation of void caused by the release of volatiles during curing and the reduced thermal stability at elevated temperatures [1].

To overcome the formation of the voids, altering the curing mechanism of PR by introducing curable groups is an extremely efficient way to avoid volatiles during the curing process. The modified PR can be cured at selective temperatures to achieve a long shelf life. Nair's work [2,3] confirmed the strategy of addition curing by introducing propargyl and ethynyl phenyl groups into phenolic systems. Based on Nair's synthesis strategy, Wang et al. [4–6] developed propargyl-containing dual-cure-mechanism PR by changing the curing mechanism to addition curing. Although addition curing could effectively avoid the formation of voids during the curing process, the residual weight of the resin at 800°C ($R_{800°C}$) was only 61%. Compared with traditional PR, the propargyl-containing PR structure has no significant advantages in terms of thermal stability.

Many elements such as B [7–9], Mo [10], Ti [11], Zr, and Si [12], can be inserted into the PR by physical blending or covalent attachment to improve their thermal stability. Si and B are widely used due to their low costs and high reactivities. Wang et al. [13] successfully introduced aryl boric acid into the PR skeleton by forming B-O-C bonds, and the char yield at 800°C was 76.4% under a nitrogen atmosphere. They systematically studied the effects of boron on the pyrolysis behavior of PR, and the results showed that the formation of B-O-C bonds reduced the content of phenolic hydroxyl groups. The existence of fewer hydroxyl groups led to a reduced the generation of free radicals, thereby decreasing the possibility of being attacked by free radicals in the pyrolysis stage. Moreover, the B_2O_3 layer was found to enrich the surface of the material and act as active oxygen and heat barriers dur-

* Corresponding author.
E-mail addresses: z.h.luo@iccas.ac.cn (Z. Luo), tzhao@iccas.ac.cn (T. Zhao).

https://doi.org/10.1016/j.polymdegradstab.2021.109599
0141-3910/

ing heat treatment from 450°C to 800°C. The enriched B_2O_3 layer provided a three-dimensional continuous oxide framework to ensure the configurational stability of the PR, endowing the boron-containing PR with better thermal stability [7,9]. However, with the increase in temperature, the damage of the boron oxide glass protective layer caused by the volatilization of boron oxide is still inevitable.

Due to the excellent comprehensive properties with organic and inorganic characteristics, Si has become another popular element that can be incorporated into the resin matrix to improve the heat resistance of PR [14]. Haraguchi et al. [15,16] introduced silicon alkoxide into PR by physical blending to enhance both the mechanical and thermal properties of PR. However, the phase separation due to the noticeable difference in solubility between PR and polysiloxanes significantly deteriorated the modified resin performance. Based on the esterification reaction between Ph-OH and Si-O-CH_3 groups, Li et al. [17] successfully inserted a functionalizing silane coupling agent into the phenolic skeleton, and they obtained a silicon modified PR with a co-continuous structure. The results showed that the hybrid resin with a co-continuous structure possessed good thermal stability and excellent flame retardance. In general, compared with physical blending, hybrid resin synthesized by covalent attachment possesses better dispersion properties and the sizes of the phase region can be controlled more effectively.

Synergistic modification with boron and silicon has shown a positive effect on improving the thermal stability of PR. In terms of thermal stability, boron oxide, with a melting point of 450°C, volatilizes significantly when the temperature increases to 800°C, while the B-O-Si bonds that connect the boron-silicate glass network are just beginning to form [18]. Therefore, the excellent overlap of the effective temperature ranges may be convincing evidence of the synergistic effects of B and Si on improving the thermal stability of PR. In the previous work of our research group, methyltrimethoxysilane (MTMS) was first introduced into PR through an esterification reaction between silicone and phenolic hydroxyl groups, and then a boron and silicon elements synergistic hybrid resin was successfully obtained by co-curing of the resin and boric acid. The char yield of this hybrid resin was improved up to 73% in a nitrogen atmosphere [19]. Furthermore, the results also revealed that boric acid could catalyze the hydrolysis of MTMS and promote the formation of a larger scale silicate network, which was beneficial for improving the thermal stability of the resin. Yun et al [20] reacted boric acid with phenolic hydroxyl groups to form B-O-C bonds, and the boric acid also served as coupling agents to react with methyltriethoxysilane (MTES) via the formation of B-O-Si bonds. The presence of B-O-C and B-O-Si bonds dramatically improved the thermal stability of the hybrid resin, and the char yield was improved up to 76% at 800°C in a nitrogen atmosphere. Their research results showed that synergistic modification with boron and silicon could effectively improve the thermal stability of PR. However, during the curing and pyrolysis procedure of the hybrid resin, no other detailed studies have been conducted on the synergistic mechanism of boron and silicon.

Based on the extensive literature described above, a combined treatment of PR involving addition curing and synergistic modification with boron and silicon has been rarely reported. In this work, boron and silicon were successfully incorporated into the PR skeleton by forming C-B-OH, B-O-C, B-O-Si, and Si-O-Ph bonds, Furthermore, addition curing was achieved via the presence of vinyl groups carried by the vinyltrimethoxysilane (VTMS). The chemical structure, curing behavior, pyrolysis mechanism, and surface morphology of the hybrid resin were studied systematically. We performed a detailed study on the synergistic effects of boron-silicon modified PR with an improved thermal stability during the curing and pyrolysis stage.

2. Experimental

2.1. Materials

4-Hydroxyphenylboronic acid (4-HBS) was purchased from Alpha Chemical Co., Ltd, Shijiazhuang, China. Anhydrous ethanol, oxalic acid, 1,4-dioxane, formalin (37 wt% of formaldehyde in aqueous solution), and ethylic acid were purchased from Beijing Chemical Factory, Beijing, China. Ethylene glycol diethyl ether and ethyl acetate were obtained from the Tianjin Chemical Reagent Co., China. Vinyltrimethoxysiloxane (VTMS) with a high degree of purity (more than 99.0%) was purchased from TCI America (Portland, OR). Novolac resin was provided by Shengquan Group Co. Ltd, Zhangqiu, China. All the reagents were used without further purification.

2.2. Preparation of hybrid resin

2.2.1. Preparation of boron-silicon-containing novolac resin (BSN)

Boron containing novolac resin (BN) [21] was synthesized by an addition-condensation reaction between 4-HBS and formaldehyde using oxalic acid as a catalyst. The 4-HBS (33.8 g, 0.2 mol) and formalin (14.41 g, 0.18 mol) were dissolved in 1,4-dioxane to a total solution volume of 100 mL in a four-necked round-bottom flask. The flask was equipped with an overhead stirrer, condenser, thermometer, and dropping funnel. After the complete dissolution of the monomer, the system was slowly heated using an oil bath and reacted at 60°C after which 0.2 g of oxalic acid was added. The temperature was increased to 95°C and held for about 8 h. After the solvent was removed under a vacuum, the remaining mixture was dissolved in ethyl acetate, followed by washing with deionized water several times until the water layer was neutral. Raw BN was obtained after the removal of ethyl acetate by rotary evaporation. The product (36.5 g) was collected and dried in a vacuum at 120°C for 48 h to ensure no water and ethyl acetate were observed.

BN (15.9 g) and ethylene glycol diethyl (50 g) were charged in a 250 mL four-neck flask equipped with a mechanical stirrer, thermometer, condenser, and dropping funnel. After the complete dissolution of BN, 0.32 g of ethylic acid was added with agitation, followed by the addition of VTMS (15.5 g) within 30 min. After this, the system was heated to 110°C and held for 6 h, then boron-silicate containing hybrid resin (BSN) (22.5 g) was obtained after the removal of ethylene glycol diethyl ether and unreacted VTMS by rotary evaporation. The BSN samples with different contents of VTMS (15.5, 10.38, 7.41 and 4.45 g) were named BSN100, BSN70, BSN50 and BSN30, respectively.

2.2.2. Preparation of cured BSN and conventional phenolic resin

BSN was subsequently cured step-wise at (120°C/2 h, 140°C/2 h, 160°C/2 h, 180°C/2 h, 200°C/2 h, and 240°C/2 h) based on the DSC analysis. As a comparison, conventional PR was also prepared. Novolac resin (21.6 g) was dissolved in ethanol (40 mL). To this solution, 2.95 g of hexamethylenetetramine was added. After the removal of the ethanol by rotary evaporation, the resin was cured according to the following procedure: 120°C/2 h, 140°C/2 h, 160°C/2 h, and 180°C/4 h.

2.3. Measurements

Fourier transform infrared spectroscopy (FT-IR) measurements were performed on a Tensor 27 spectrometer by using KBr disks at the ambient temperature. ^{1}H-NMR, ^{11}B-NMR, and ^{29}Si-NMR spectra were recorded on a Bruker Advance 400 MHz NMR spectrophotometer. Solid-state NMR experiments were performed on a Bruker standard-bore 11.7 T ($\nu 0(1H) = 400$ MHz) NMR spectrometer equipped with a Bruker Advance III console and with a

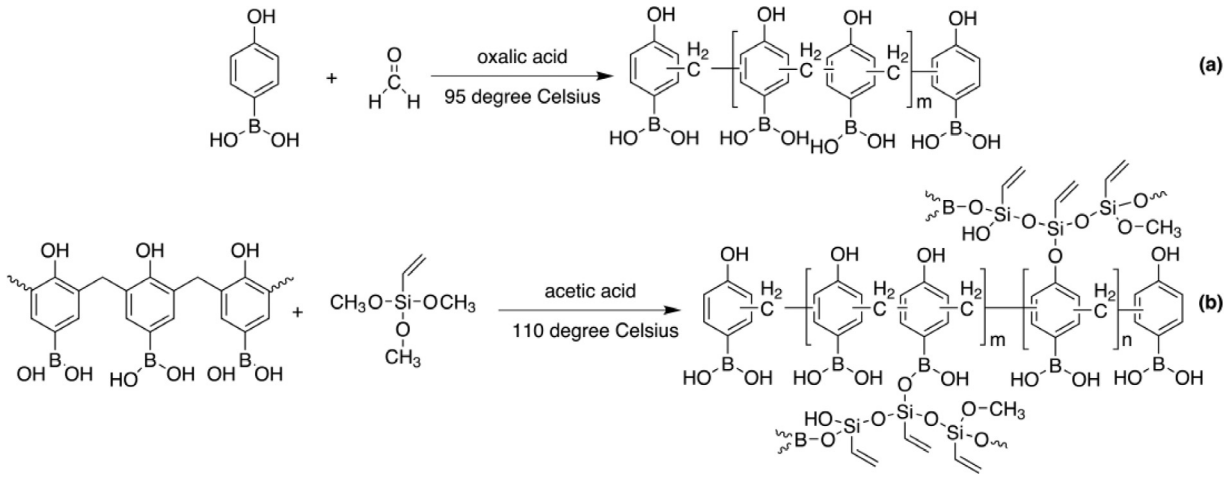

Fig. 1. Synthesis route for boron-silicon-containing novolac resin (BSN): (a) addition condensation reaction and (b) esterification reaction.

Bruker 4 mm broad-band HX MAS probe. Simulations of all MAS ^{11}B solid-state NMR spectra and ^{29}Si solid-state NMR spectra were performed in the solid line shape analysis (SOLA) module v2.2.4 included in the Bruker Topspin v4.0.1 software. Gel permeation chromatography (GPC) analysis was performed using a Waters Instrument (515 HPLC pump, 2410 refractive index detector) using tetrahydrofuran as the eluent and polystyrene as the standard for calibration. Differential scanning calorimetry (DSC) was performed on a Mettler Toledo DSC 822e over the range from 30 to 400°C at a heating rate of 10°C/min in nitrogen. Thermo gravimetric analysis (TGA) was carried out from the ambient temperature to 900°C on a NETZSCH STA 409PC at a heating rate of 10°C/min in nitrogen, respectively. The surface morphology of the hybrids was observed on a Hitachi S-4800 scanning electron microscope (SEM) at an accelerating voltage of 10 kV. Energy dispersive X-ray spectroscopy (EDX) was performed on an Oxford INCAx-sight 7593 system attaching to the SEM apparatus. X-ray photoelectron spectroscopy (XPS) measurement was performed using an ESCALAB250XI instrument. The Raman spectra were recorded on a Renishaw inVia plus using the 633 nm excitation line of an Argon-ion laser. On-line testing of gaseous products obtained during the thermal pyrolysis was performed using a thermogravimetric analyzer (NETZSCH STA 409FC Germany) coupled with a Fourier transform infrared spectrometer (Bruker Tensor 27 Germany) and a mass spectrophotometer (NETZSCH QMS 403 Germany). The X-ray diffraction (XRD) patterns were recorded using a Rigaku D/MAX2400 with Cu Kα radiation (λ=0.154 nm, 40 kV and 40 mA) to examine the structural evolution of the pyrolysis products.

3. Results and discussion

3.1. Synthesis and characterization of BSN

The synthesis of BSN was conducted in two steps (Fig. 1). First, 4-HBS was used as a monomer to react with formaldehyde to incorporate B, and the feeding ratio was set as 0.9 to obtain a boron-containing novolac resin (BN). In this work, 4-HBS with three functional groups, including two boron hydroxyl groups and one hydroxyl group, was selected both as a phenol source to react with formaldehyde and a boron source to facilitate the formation of the three-dimensional cross-linked structure by the B-O-B and B-O-C bonds. Second, based on the esterification reaction between the Si-O-R with the hydroxyl groups of 4-HBS, VTMS was attached to the molecule of the as-obtained BN by forming Si-O-Ph and Si-O-B bonds. Finally, the BSN was successfully obtained.

The chemical structures of the BSNs were examined by FT-IR and NMR. Fig. 2a shows the FT-IR spectra of the BSN resin. The characteristic absorption bands of the benzene ring were observed at 1610-1596 cm^{-1}, and the peak at 1232 cm^{-1} corresponded to the stretching vibration of the C-O structure of the phenolic hydroxyl groups. The Si-O-Ph signal [19] at 946 cm^{-1} was formed after the esterification reaction between BN and VTMS, confirming that the silicon source had been successfully introduced into the resin skeleton though Si-O-C bonds. The peak at 1350 cm^{-1} corresponded to the stretching vibration of the B-O structure on the B-O-C [13] structure in the 4-HBS. Meanwhile, the peak at 890 cm^{-1} was attributed to the stretching vibrations of B-O in the B-O-Si structure [18,22], which indicated that boron and silicon were simultaneously introduced into the hybrid resin via the formation of B-O-C, Si-O-C, and Si-O-B bonds. Three sharp peaks at 1410 and 1010 cm^{-1} could be attributed to the Si-CH=CH$_2$ [23,24]. The absorption peaks at 1440 and 1276 cm^{-1} were attributed to the stretching vibrations of B-C [25] in the Ph-B structure and Si-CH in the Si-CH=CH$_2$ [24] structure. The peaks at 1000-1200 cm^{-1} were assigned to Si-O-Si absorptions. The 1114 cm^{-1} band was assigned to the symmetric structure (cage-open cage), whereas the 1080 cm^{-1} band was assigned to the random network structure [26,27]. The splitting of the peak verified the different hydrolysis degrees of the VTMS [28].

The ^{1}H-NMR(DMSO-d6) spectrum of BSN100 is shown in Fig. 2b. The broad peak at 3.5-4.0 ppm was assigned to the bridging -CH$_2$- between the phenol rings, confirming that the addition-condensation reaction occurred between 4-HBS and formaldehyde. Chemical shifts between 9.36 and 9.18 ppm were assigned to the hydroxyl hydrogens on the phenol ring. The signals at 8.0-7.8 ppm corresponded to B-OH in the 4-HBS, and that at 7.4-6.5 ppm was assigned to the aromatic protons. The broad peaks at 6.2-5.7 ppm were attributed to the -CH=CH$_2$ in the VTMS structure, and those at 3.60 and 3.17 ppm were assigned to the unreacted -Si-O-CH$_3$ of the VTMS (T1, T2, and T3) [29], The signal at 2.5-0.8 ppm corresponded to the solvent peak.

^{11}B and ^{29}Si-NMR (Fig. 2c and d) were applied to confirm further the chemical state of the boron and silicon in the BSN100 skeleton. The ^{11}B NMR (Fig. 2c) measurements were carried out to obtain environmental information of the B species in the BN. In the ^{11}B NMR spectrum, the presence of a chemical shift at 29 ppm (B1) are attributed to B-O-B and B-O-C structures. The 26 ppm (B2) was attributed to the Si-O-B structure [25,30,31]. In the ^{29}Si-NMR (Fig. 2d), three peaks appeared at -80.27 ppm (T3, intense peak), -

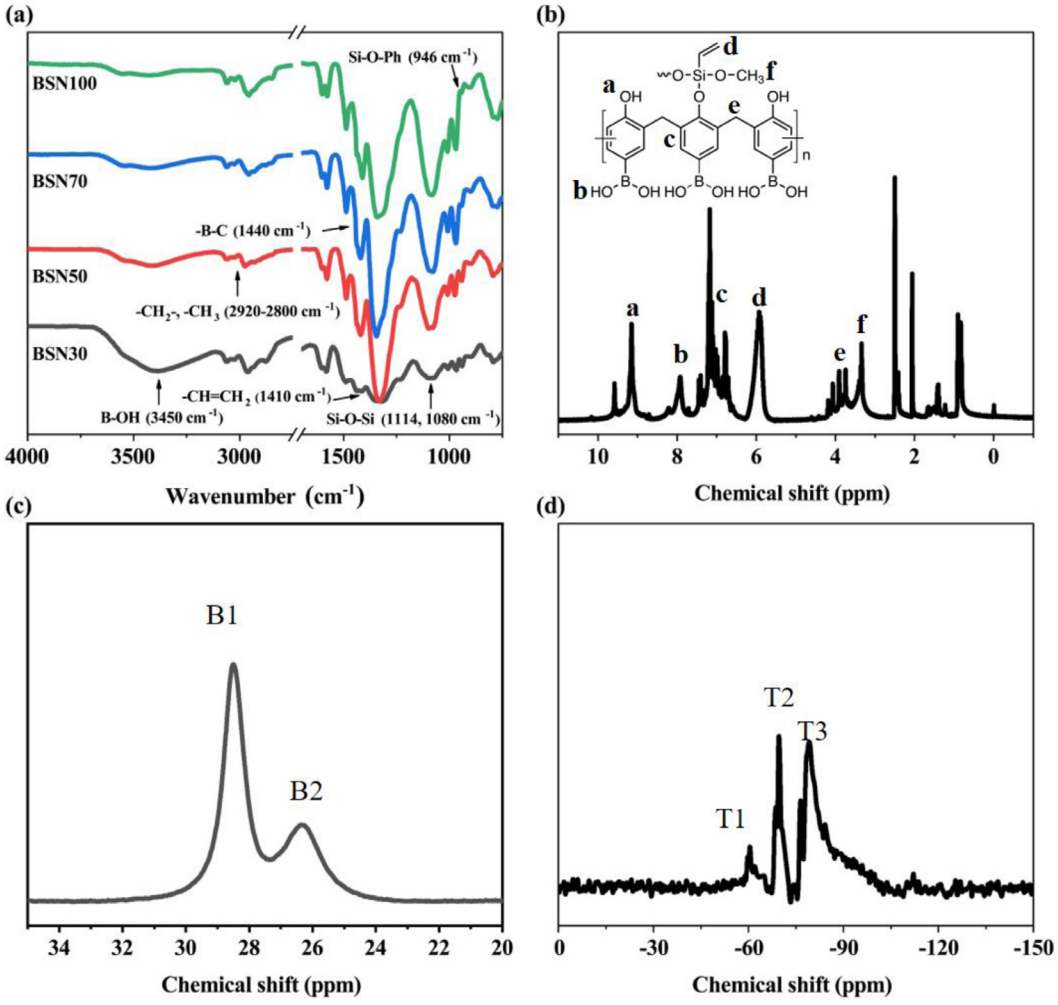

Fig. 2. Structural characterization of BSNs: (a) Fourier-transform infrared spectroscopy (FT-IR) spectra, (b),^{1}H-NMR (nuclear magnetic resonance) spectra, (c) ^{11}B-NMR spectra, and (d) ^{29}Si-NMR spectra.

71.49 ppm (T2, medium peak), and -59.33 ppm (T1, low peak) [32]. In all cases, T1, T2, and T3 were derived from silicon with three, two, and one Si-O-Si bridges, respectively, and at least one organic group.

In-situ ^{29}Si-NMR spectroscopy was employed to obtain more key information to elucidate the chemical reactions. We explore and develop a approach for performing in situ ^{29}Si-NMR spectroscopy to study complex reaction systems. As shown in the Fig. 3a, by adjusting the flow rate of the peristaltic pump, the reaction liquid is pumped into a specially designed nuclear magnetic tube in real-time, and the in-situ silicon spectrum (Fig. 3b) can be obtained through the cooperation of several devices.

In the time evolution of the ^{29}Si-NMR spectrum of the reaction of BSN100, three peaks observed at -80.27 ppm (T3), -71.49 ppm (T2), and -59.33 ppm (T1). After 6 h of the reaction, the intensity of the T1 peak decreased sharply, and the intensities of the T2 and T3 peaks began to increase at about 0-3 h. At this time, although T2 began to slowly decrease, the T3 peak continued growing. The intensities of all the peaks did not change significantly from 5.5 h to the end of the reaction. The results showed that during the progress of the reaction, the T1 structure continued to transform into the T2 and T3. The reaction began to slow at about 3 h and ended after 5.5 h. No raw material peak (VTMS -52.1 ppm) was found in the BSN resin system, demonstrating that all the VTMS was involved in the second step of the well-designed reaction.

Table 1
Molecular weight of the BSNs determined by GPC.

System	M_n	M_w	M_w/M_n
BSN30BSN50	472529	613726	1.301.37
BSN70	565	825	1.46
BSN100	623	956	1.53

Thus, it can be confirmed that the NMR results were highly consistent with those of FT-IR.

GPC was employed to determine the molecular distribution characteristics of the BSNs, including the number average molecular weight (Mn), weight average molecular weight (Mw), and polydispersity index (PI). As shown in the molecular distribution profiles (Fig. 4), the peak intensities attributed to the low and middle molecular weight components continue to decrease and the high molecular weight components increase with the increase in the VTMS content. Table 1 presents the values of Mn, Mw and PI of the BSNs. those values increased with the increased VTMS content, revealing that the esterification reaction between the VTMS and PR was carried out successfully.

Overall, the molecular structures of the BSNs were characterized by several spectra, including ^{1}H-NMR, FT-IR, ^{11}B-NMR, and ^{29}Si-NMR spectra, and the results confirmed that addition-curable boron-silicon containing hybrid resin was prepared successfully.

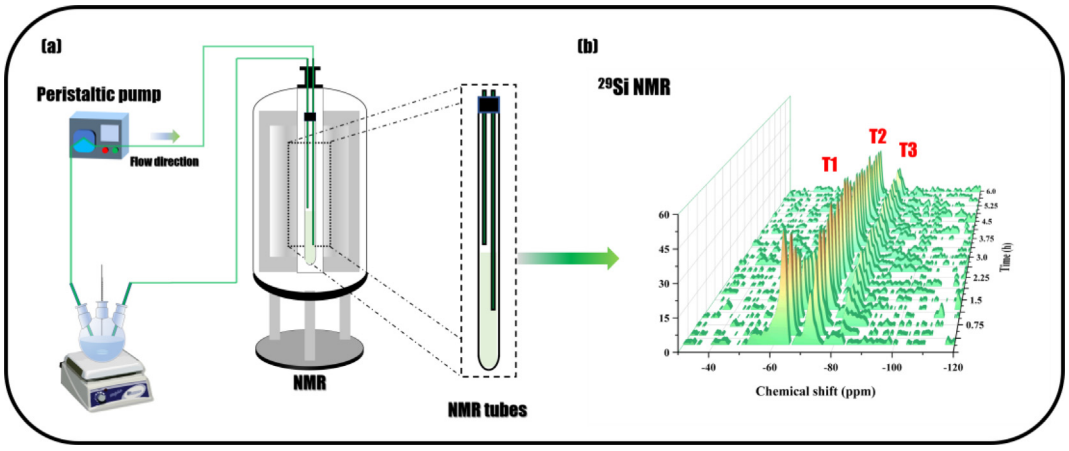

Fig. 3. (a) In-situ ^{29}Si-NMR spectrogram acquisition device. (b) Time evolution of the ^{29}Si-NMR spectrum of the reaction of BSN100.

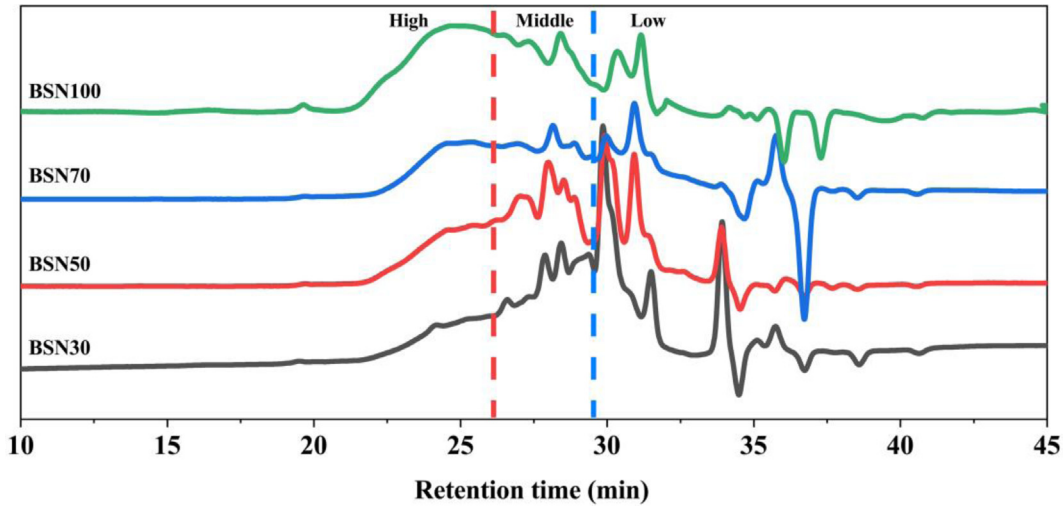

Fig. 4. Gel permeation chromatography (GPC) curves of the BSNs.

3.2. Curing behavior of BSN

The curing behavior of the BSN was examined by DSC (Fig. 5a). The DSC curves exhibited an exothermic peak at the temperature range of 160°C -280°C with a peak value of about 235°C. Moreover, with the increased content of VTMS, the exothermic peak became sharper, revealing that a higher VTMS content led to a more vigorous curing reaction. Based on the DSC results, a reasonable curing procedure was designed as follows:

120°C, 1 h → 140°C, 1 h → 160°C, 2 h → 180°C, 2 h → 200°C, 2 h→ 240°C, 2 h.

Although the exothermic peak was a simple singlet, the complicated molecule structure of the BSN suggested that the exothermic peak could have been due to complex reactions. Therefore, a more detailed FT-IR characterization at the different heating stages was carried out to monitor the progress of the curing reactions, and the detailed results are shown in Fig. 5b. There was almost no change in the FT-IR spectrum during the curing process as the temperature reached 160°C. As the curing reaction reached 180°C, the decrease in the B-C signal (1440 cm^{-1}) indicated that the binary boron structure (HBS) transitioned into a trigonal boron structure (boron oxide). The center of the infrared absorption peak of the B-O bond vibrations shifted from 1350 to 1380 cm^{-1}. The characteristic peaks at 1350 cm^{-1} and 1380 cm^{-1} were reported in the literature [13, 20] and interpreted as the stretching vibration of B-O-C bonds in 4-HBS and boron oxide demonstrated a more heat-resistant continuous B-O-B and B-O-C network gradually formed at the elevated temperature. The absorption at 890 $cm^{-1,}$ which was attributed to the B-O-Si structure, maintained a strong signal intensity after the heat treatment. However, after the curing temperature exceeded 160°C, the intensity of the Si-O-Ph (946 cm^{-1}) signal became much weaker. The peaks at 1000-1200 cm^{-1} are assigned to Si-O-Si absorption. The 1095 cm^{-1} band was attributed to the symmetric structure, whereas the 1079 cm^{-1} band was assigned to the random network structure. Fundamentally, the different positions of the bands depended on the degree of cross-linking and the physical structure of silica [26,27]. The splitting of the Si-O-Si peak near 1100 cm^{-1} gradually became a single peak with a shoulder, suggesting that the improvement of the hydrolysis degree of the VTMS promoted a larger scale Si-O-Si network in the presence of boric acid. Furthermore, the size of the absorption peak of vinyl (1410 cm^{-1}) dramatically decreased, and an absorption peak at 1255 cm^{-1} corresponding to the Si-CH_2- stretching vibration [33] began to appear. These results indicated that the addition of the curing reaction between the vinyl groups occurred successfully.

^{11}B solid NMR (Fig. 12a-1) measurements were carried out to obtain environmental information of the B species in the cured BSN, which could be used as a complementary tool to FT-IR. Peak deconvolution of the ^{11}B solid NMR spectrum of the cured BSN into six peaks with chemical shifts at ca.24, 18, 15, 11, 2, 0, and -2.8

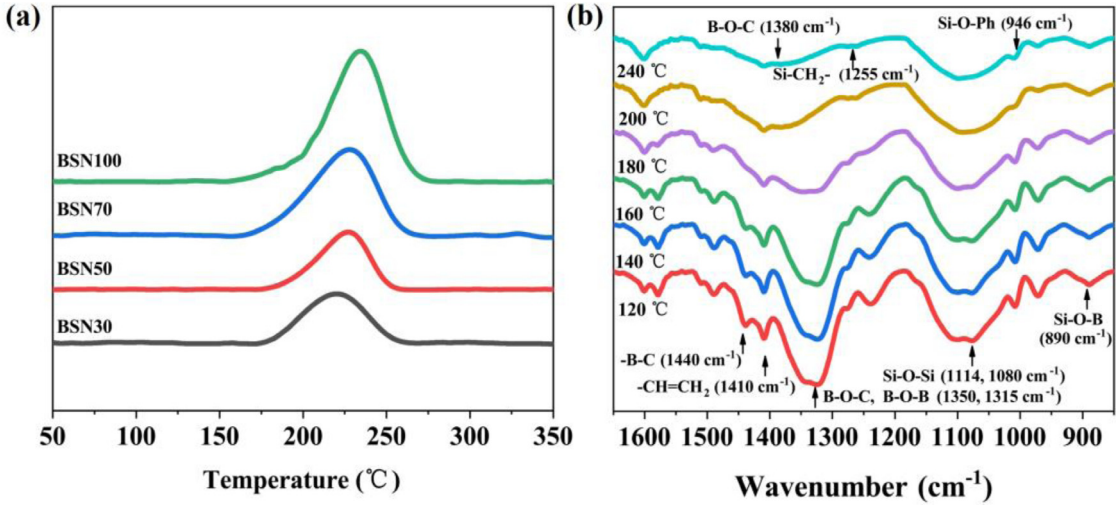

Fig. 5. Studies of curing behavior of the BSNs:(a) differential scanning calorimetry (DSC) curve, and (b) FT-IR spectrum of the BSN resin.

ppm was performed. The presence of a chemical shift at 24 ppm was assigned to B-O-Si in the 4-HBS, and the chemical shifts at 18, 15, and 11 ppm were ascribed to tri-coordinated boron. Furthermore, the peaks at around 2, 0 and 2.8 ppm were accordingly assigned to B $(OH)_1(OSi)_3$, $B(OH)_2(OSi)_2$ and $B(OSi)_4$ tetrahedral framework. Normally, the ^{11}B isotropic chemical shift of trigonal boron correlates with the number of hydroxyl groups on the B atoms, and the peak at 18 ppm is often attributed to $B(OH)_3$. Sites B [3]^b and B [3]^c belong to the framework $B(OSi)_xOH_{3-x(x\ =\ 1,2)}$ and the $B(OSi)_3$ structure [34–38]. The binary boron structure (4-HBS) transitioned into a trigonal boron structure (boron oxide), consistent with the FT-IR results. The trigonal boron structure and the B-O-Si bonds that formed from the esterification reactions between the B-OH and Si-O-CH_3 [22] were beneficial for improving the thermal resistance of the resin system.

The ^{29}Si NMR measurements have also been carried out to obtain useful environmental information about the Si species in the cured BSN. ^{29}Si NMR of the cured BSN (Fig. 12b-1) showed three peaks at -80.53, -71.49, and -60.00 ppm. Compared with Fig. 2d, the percentage of the integral area of T_3 units increased significantly, indicating that the hydrolysis degree of VTMS.

A core-level XPS measurement was performed to determine the chemical states of the elements on the surface of the cured BSN. The carbon, oxygen, boron, and silicon peaks were detected from the full scanned XPS spectrum of the cured BSN100 (Fig. 10a-1). Fig. 10-b-1 represents a high-resolution B1s XPS spectrum. The binding energy centered at 192.0, 192.9, 193.5, and 194.5 eV was ascribed to B-O-C, B-O-B, B-O-Si, and B-OH bonds, respectively [20] The main components of the Si2 peak (Fig. 11c-1) at 102.2 eV were attributed to the Si-O-B structure. Thus, the results obtained by XPS and ^{29}Si-NMR were in line with the results obtained by FT-IR.

Based on the above analysis, we can convincingly distinguish three main chemical reactions that occurred in the whole curing process:

(i) the addition-curing of VTMS;
(ii) the formation of a larger-scale continuous B-O-B network;
(iii) the formation of a larger-scale continuous Si-O-Si network.

Boron, silicon, and carbon atoms have similar atomic radii and electronegativities, making it possible for carbon and boron atoms to replace silicon in the Si-O-Si structure. Furthermore, both B-O-B (516 kJ/mol) [13] and Si-O-Si (446 kJ/mol) [33] with intense bond energies and excellent thermal stability, tended to form a three-dimensional continuous oxide frameworks. By connecting B-O-C, B-O-Si, and Si-O-C bonds, the oxide framework and cured PR skeleton were firmly bonded together, endowing the hybrid resin with excellent thermal stability. Based on the above discussion, and to make this article more rigorous, the possible molecule structures of the cured BSN are shown in Fig. 6.

Table 2
TGA results for cured BSN resin and conventional PR.

Sample	Weight loss temperature (°C)			$R_{800°C}$ (%)
	$T_{5\%}$ (°C)	$T_{10\%}$ (°C)	T_{dmax} (°C)	
PR	410.21	478.47	540.14	60.21
BSN30	375.35	500.62	576.21	69.53
BSN50	400.38	521.29	578.35	72.14
BSN70	411.37	532.27	593.46	76.34
BSN100	458.56	582.06	611.05	81.02

3.3. Thermal properties of cured BSN

TGA was applied to evaluate the thermal properties of the cured BSNs with different contents of VTMS during pyrolysis, especially between 300°C and 700°C, and the DTG was used to characterize the maximum decomposition temperature and maximum decomposition rate of the resin systems. The cured BSNs with different VTMS contents had extremely similar thermal decomposition behaviors. Thus, the cured BSN100 with the highest residual weight was chosen to investigate the thermal properties and thermal degradation behavior.

The corresponding data are shown in Table 2. Fig. 7a clearly shows that the initial thermal degradation temperature ($T_{5\%}$) of the cured BSN100 was 458.56°C under an N_2 atmosphere, which was increased by 11.1% compared to that of the PR, and the residual weight at 800°C ($R_{800°C}$) was as high as 81%, which was 33.8% higher than that of the PR. From the DTG curves (Fig. 7b), the maximum thermal decomposition temperature of BSN100 was 611.05°C under an N_2 atmosphere, which was higher than that of PR. Meanwhile, the maximum decomposition rate of the BSN was 0.099%, which was reduced by 41% compared with the value of the PR, suggesting the excellent thermal stability of the BSN.

3.4. Thermal pyrolysis behavior of cured BSN

To more clearly investigate the reason that the BSN100 had such excellent residual weight (81.02%), the TG-MS-FT-IR technique

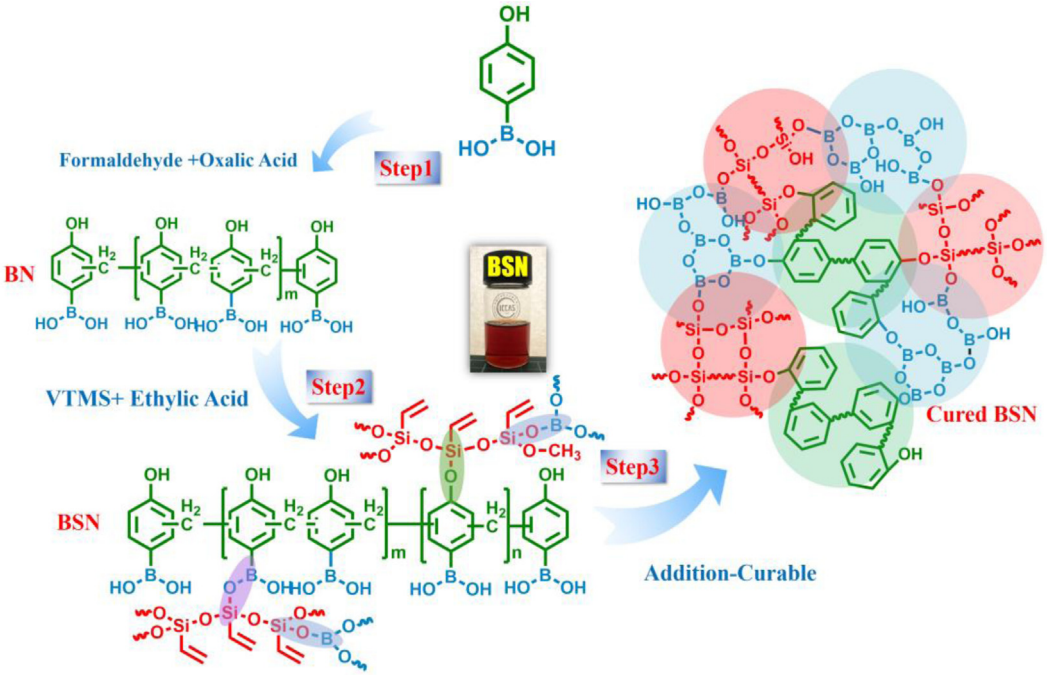

Fig. 6. Possible structure and curing mechanism of BSN resin.

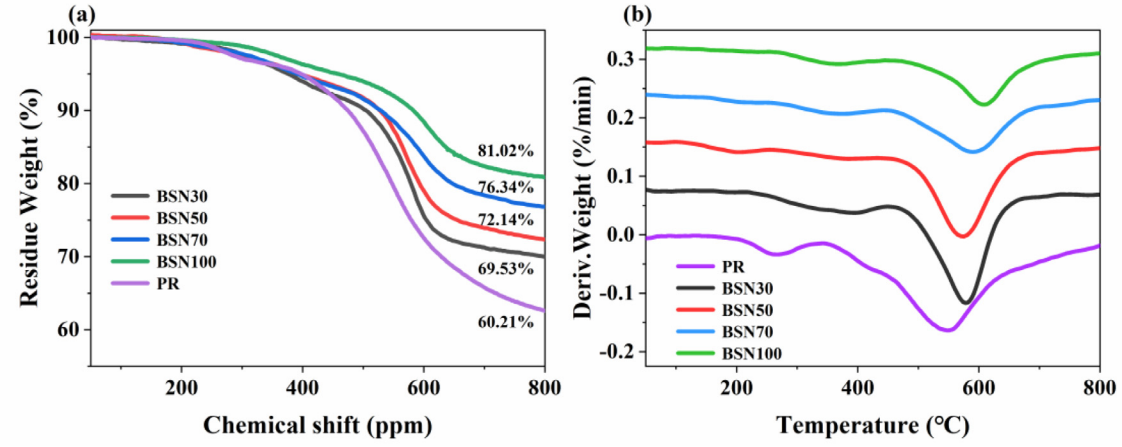

Fig. 7. Thermal analyses of cured BSNs and PR under N_2 atmosphere: (a) thermogravimetric analysis (TGA) curves and (b) derivative thermogravimetry (DTG) curves.

was applied to evaluate the detailed volatile products and gather useful information to investigate the exact thermal pyrolysis reactions along with the polymer stability under controlled conditions.

The two-dimensional FT-IR contour maps of the gaseous products of the BSN resin pyrolysis are shown in Fig. 8a and S1. The detailed FT-IR diagram of the gaseous products at several representative temperatures [39] is shown in Fig. 8b. In Fig. 8a and b, the first thermal degradation stage between 200°C and 450°C was mainly attributed to the release of water, phenol, and unreacted small molecule monomers. The peaks corresponding to phenol (m/z = 94), boric anhydride (m/z = 106), and dimethoxy(vinyl)silanol (m/z = 134) in Fig. 8d-250°C are a good illustration of this. In addition, the release of H_2O indicated that condensation reactions occurred among B-OH, Si-OH, and phenolic hydroxyl groups, facilitating further intermolecular cross-linking. As the temperature increased from 450 to 800°C, the appearance of new peaks at mesitylene (m/z = 120), naphthalene (m/z = 128), 2,4,6-trimethyphenol (m/z= 136), O-xylene, P-xylene (m/z = 106) and methanone (m/z = 209) in the Fig. 8d-600°C confirmed that the cross-linked network of PR underwent an irreversible rearrangement and formed polyaromatic domains [40]. Simultaneously, the infrared spectra at B-O (1350 cm^{-1}) and Si-O (1178 cm^{-1}) showed a dramatic change in the peak intensities. As shown in Fig. 8c, B_2O_3 with a low melting point of 450°C was quickly removed from the hybrid materials via the endothermic volatilization process when the temperature reached 600°C. Therefore, B-O (1350 cm^{-1}) exhibited a powerful infrared absorption during pyrolysis with the temperature reached 600°C. Meanwhile, the intensities of the Si-O (1178 cm^{-1}) vibrations showed a considerable increase at 600°C and dropped sharply as the temperature increased to 1000°C. This result implicated that heat treatment at 600°C caused significant breakage of the weak edge Si-O-Si bonds, which led to the volatilization, degradation, and dissolution of small silicon-containing molecules. Nevertheless, a higher temperature also enhanced the reactivity of silicate [41], which resulted in a large-scale continuous Si-O-Si network with excellent thermal stability. The network was rarely destroyed under the sustained heat treatment from 600°C to 1000°C.

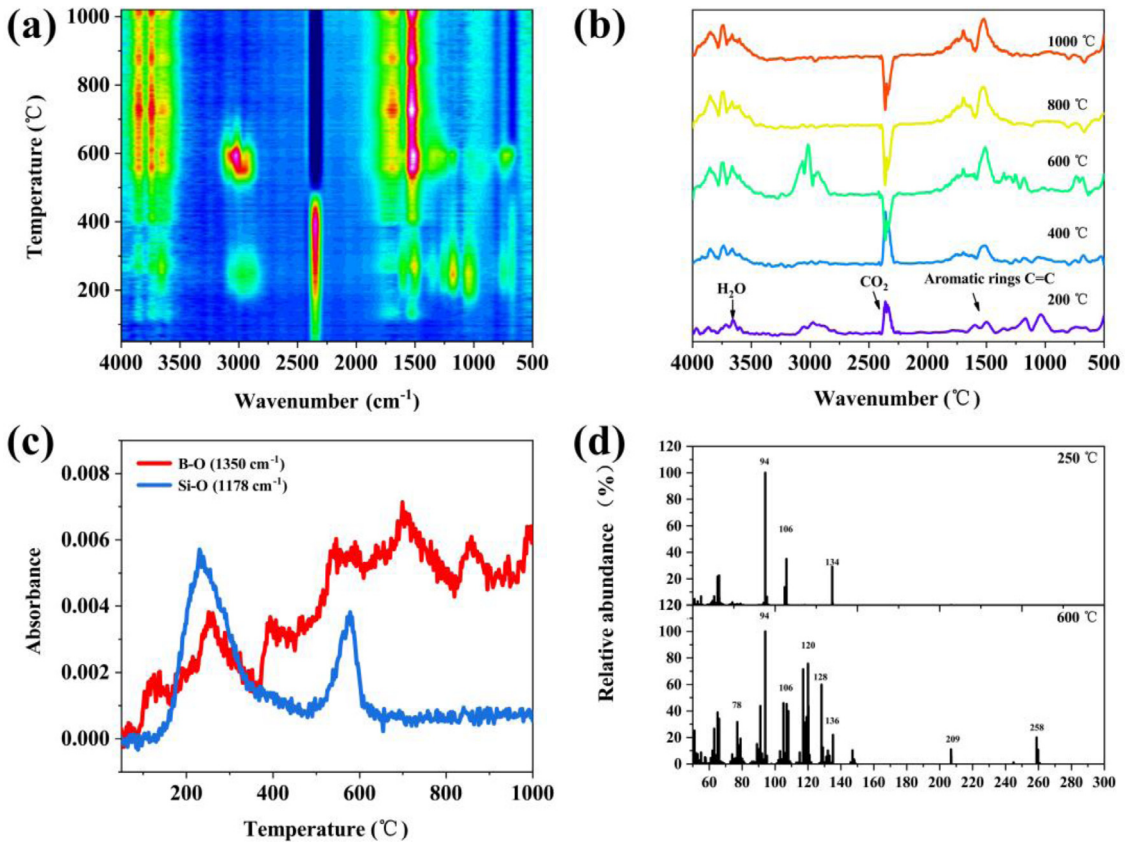

Fig. 8. Thermal degradation behavior of the BSN100: (a) two-dimensional FT-IR diagram of volatile product, (b) FT-IR spectrum, (c) between intensity and temperature for B-O (1350 cm^{-1}) and Si-O (1178 cm^{-1}), and (d) mass spectrum (MS).

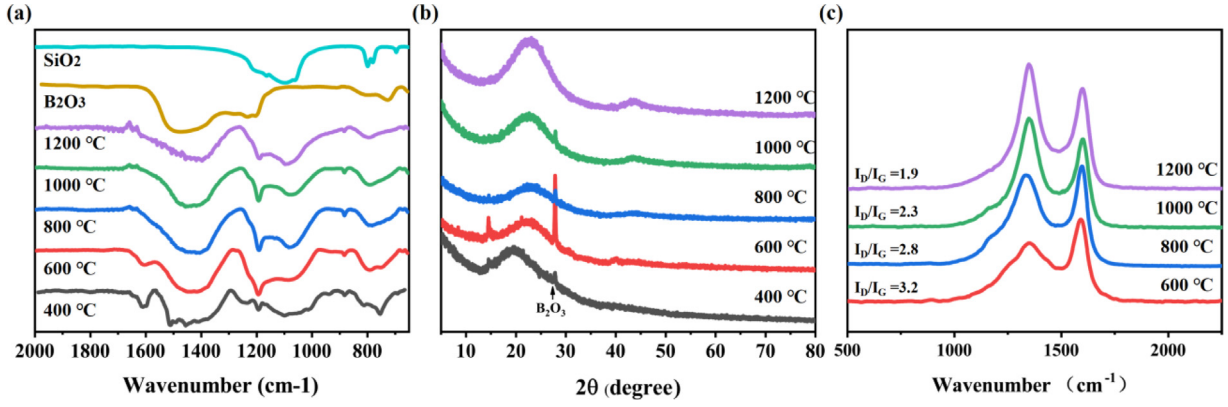

Fig. 9. Chemical structure changes of the carbonization product of the BSN100: (a) FT-IR spectrum, (b) X-ray diffraction (XRD) spectrum, and (c) Raman spectrum of the BSN100 at different temperatures during the pyrolysis stage.

After the above analysis, the following preliminary conclusions about the thermal pyrolysis reactions along with the polymer stability can be drawn:

(i) The release of a large amount of water further enhanced the condensation reaction among the B-OH, Si-OR, and Ph-OH, facilitating the formation of further intermolecular cross-linking structure.
(ii) Exposure at high temperatures (>600°C) promoted a deep-seated rearrangement of the BSN carbon skeleton and polyaromatic domains with excellent heat resistance.

Next, the structural characterization of the carbonization products of the BSN100 was carried out to verify the above conclusions. FT-IR was been used to investigate the chemical structural changes of the hybrid resin during pyrolysis. As shown in Fig. 9a, the number of characteristic absorption peaks of the sample decreased as the temperature increased to 1200°C. The absorption peaks centered at around 1500-1300 cm^{-1} and 1200-1000 cm^{-1} corresponding to the B-O-B and Si-O-Si structures, respectively, shifted toward the characteristic peaks of inorganic boron oxide and silica oxide. These shifts indicate that an intermolecular cross-linking structure formed by oxygen-containing groups promoted a larger-scale cross-linked networks of B-O-B and Si-O-Si. Meanwhile, the XRD pattern (Fig. 9b) showed a crystalline diffraction peak from B_2O_3 at $2\theta = 28.1°$, which was consistent with the FT-IR results. Furthermore, the band at 890 cm^{-1} ascribed to the absorption of Si-O-B bonds was always present during the heat treatment, indicating that boron oxides and silicon oxides were not a simple phys-

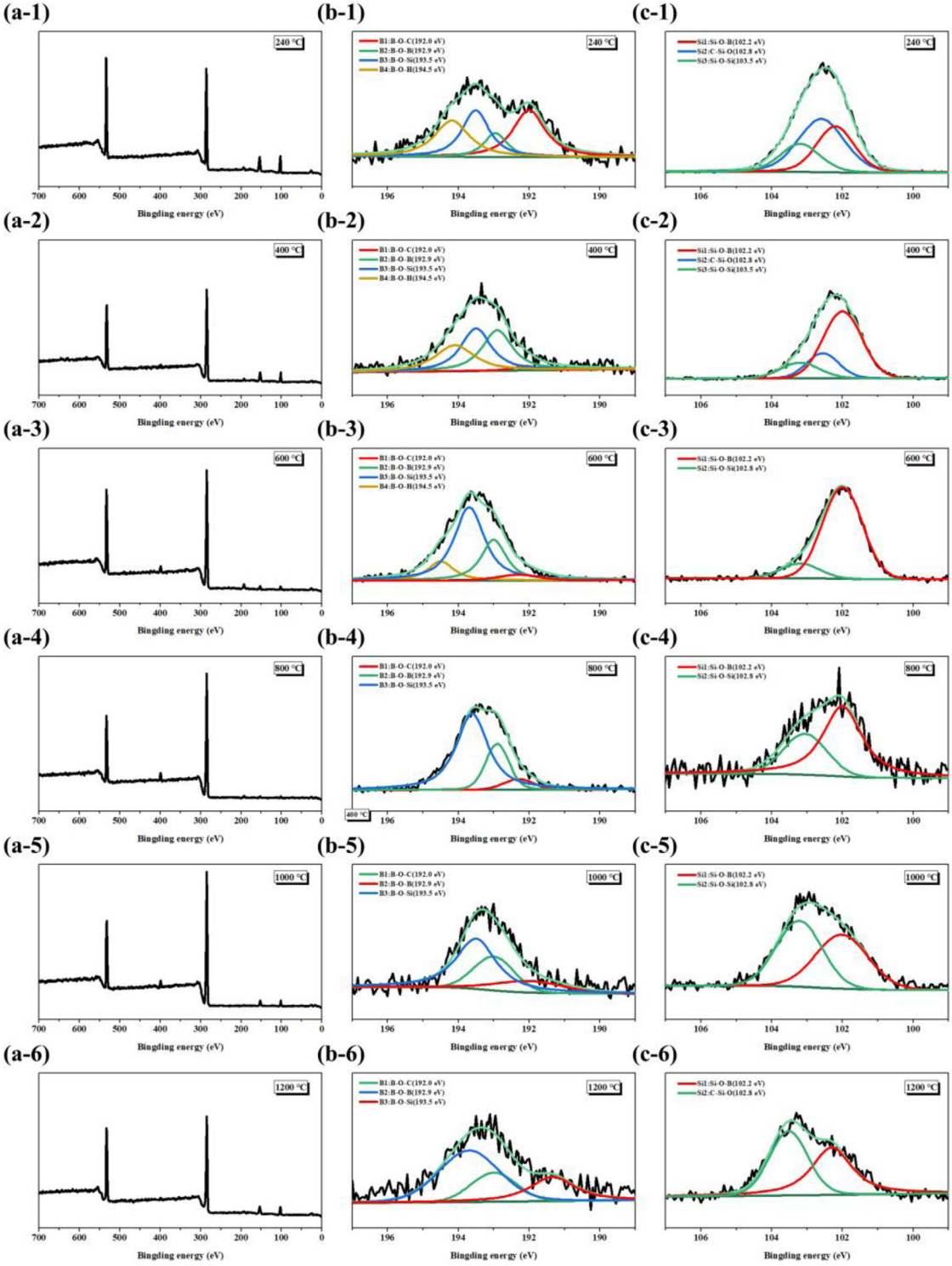

Fig. 10. X-ray photoelectron spectroscopy (XPS) spectra of the BSN100 at different temperatures during pyrolysis stage: (a) a full-scan, (b) B_{1s}-XPS spectrum, and (c) Si_{2p}-XPS spectrum.

ical mixture. Therefore, there were strong interactions between B-O-B and Si-O-Si networks through the formation of Si-O-B bonds. It was concluded that the formation of a higher degree of the B-O-B-O-Si-O-Si continuous oxide framework during the thermal pyrolysis endowed the hybrid resin with remarkable thermal stability and was especially conducive to the high residual weight of BSN.

XRD and Raman spectroscopy were applied to determine the structural characteristics of the carbonaceous material obtained at different temperatures. As shown in Fig. 9b and c, the average crystallite dimensions L_c (002), L_a (100) and d_{002} were calculated using the Scherrer and Bragg equations [42], and their values were 9.47Å (L_c), 19.01Å (L_a), and 3.88 Å (d_{002}), respectively. In the Raman spectra, the D-band (nearly 1358 cm^{-1}) was mainly associated with disordered carbon and amorphous carbon, and the G-band (approximately 1580 cm^{-1}) was assigned to the ordered graphitic structures. The intensity ratio ($I_R = I_D/I_G$) of the D and G bands

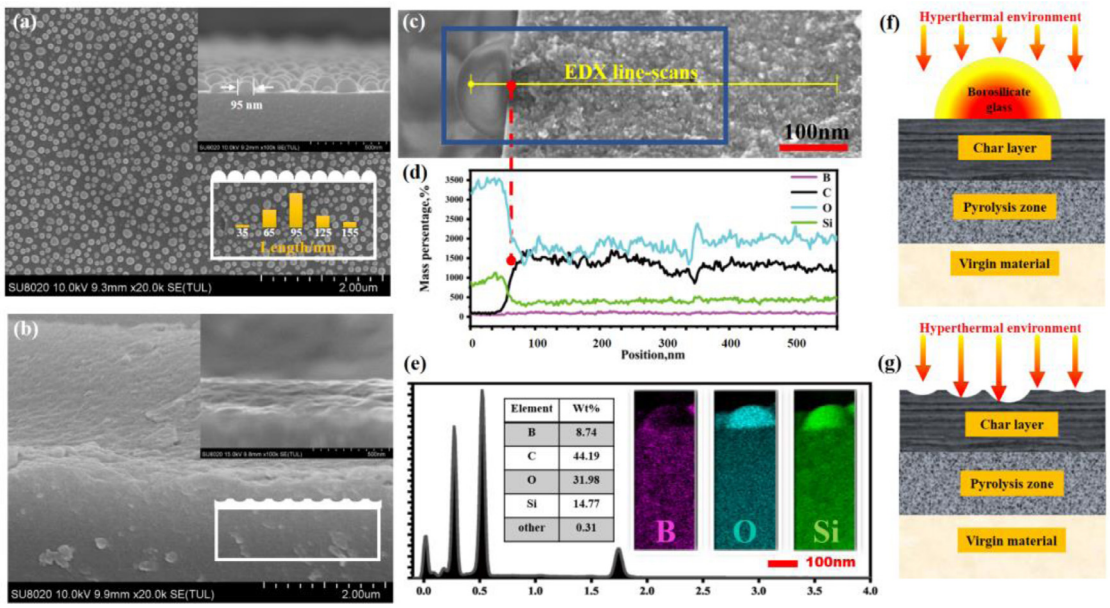

Fig. 11. Characterization of the BSN100 after the pyrolysis process: (a) scanning electron microscopy (SEM) image of cured BSN100 after treatment at 800°C in N_2 (a), (b) the SEM image of cured PR after treatment at 800°C in N_2, (c) the (c-e) SEM- dispersive X-ray spectroscopy (EDX) line-scans of cured BSN100 after treatment at 800°C in N_2, (f, g) structure diagrams of carbonization product of cured BSN100 and PR after treatment at 800°C.

is associated with the order of carbon materials. The lower the I_R value is, the higher the degree of the transformation from disordered carbon to graphitic carbon is. As shown in Fig. 8d, the I_R decreased from 3.2 to 1.9 as the temperature increased.

An extensive literature review was undertaken to understand the carbon structure derived from the pyrolysis process of the cured phenolic resin (CCPR). CCPR were gradually transformed into a more heat-resistant, finite-sized, polyaromatic structure as the temperature increasing [13,43,44]. The finite-sized stacks of polyaromatic structures as the basic structural units (BSU) of CCPR were stacked on top of each other to form a carbon skeleton. The carbon skeleton and some inaccessible pores between the BSU stacks constitute the basic structure of the CCPR [44]. The possible structure of the CCPR is shown in Fig. 13a.

Based on the above discussion, we have characterized the polyaromatic orderliness of the carbonized product structures during pyrolysis; simultaneously, XPS was used to determine the various combinations of boron and silicate of the surface on the carbonization production. The statistic obtained by fitting the XPS spectrogram (Fig. S2a) clearly shows that the contents of boron and oxygen inside the carbonized product increased as the temperature increased.

When the pyrolysis treatment was between 400°C and 800°C, boron and oxygen were enriched constantly on the surface of the carbonization. Furthermore, the result of the XRD obtained by the same carbonization indicated the existence of B_2O_3. Jing et al. described the B_2O_3 layer enrichment of the surface of the material, which acted as active oxygen and heat barriers during heat treatment from 450°C to 800°C [13]. The preliminary results described above were in agreement with previously reported results. When the temperature increased further, the high temperature aggravated the volatilization of B_2O_3 located on the surfaces of the materials. Meanwhile, the silicate with better heat resistance gradually migrated to the surface of the material.

The corresponding B_{1s} and Si_{2p} high-resolution deconvoluted XPS spectra were obtained to identify the elements on the surfaces of the carbonization products and determine their chemical states and binding characteristics. In addition, the deconvoluted peaks could be compared to the core-level binding energy peaks found in reference databases [20] and to provide percentage of each species as a function of each element. As shown in Fig. 10b and Fig. S2a, b, and c. the binding energy centered at 192.0, 192.9, 193.5, and 194.5 eV can be ascribed to B-O-C, B-O-B, B-O-Si, and B-OH bonds, respectively. The disappearance of the peak belonging to B-OH suggested that higher temperatures facilitated further condensation reactions between the B-OH, Si-O-R, and Ph-OH and enhanced the cross-linking density of the resin. The greater the cross-linking density was, the better the heat resistance became. Simultaneously, the increasing intensity of the peak ascribed to the B-O-C structure attracted our interest. Previous literature [45, 46] showed that at elevated temperatures, the terminal oxygen atoms of glassy B_2O_3 could be bonded to the chemically unstable carbon atoms of graphite, which resulted in a marked reduction in the rate of oxidation of the graphite in dry or moist air between 600°C and 1000°C. Meanwhile, the results discussed above showed that the carbon structures in PR were gradually transformed into a more heat-resistant ordered polyaromatic structure as the temperature increased. The existence of the ordered polyaromatic structure promoted the graphitization of the pyrolysis products [13]. Therefore, the formation of the B-O-C structure may have been closely related to the ordered polyaromatic structure derived from the BSN. At 1200°C, the chemical states of the B atoms inside the materials were composed of B-O-C, B-O-Si and B-O-B structures, endowing the resin with excellent thermal stability.

The results of the high-resolution Si_{2p} [47] deconvoluted XPS spectrum showed that when the temperature reached 400°C, the decreased intensity of the C-Si-O signal indicated that the structure of the silicon atoms evolved from silicon units bearing three oxygen atoms and one carbon atom (denoted as $[SiO_3C]$) to silicon units bearing four atoms (denote as $[SiO_4]$), which thereby increased the possibility of formation of Si-O-Si structures and facilitated the formation of a further intermolecular cross-linked structure during the heat treatment. Moreover, the existence of the B-O-Si structure not only was highly consistent with the results of the FT-IR and B_{1s} XPS spectrum but also indicated that the high temperature improved the formation of a three-dimensional con-

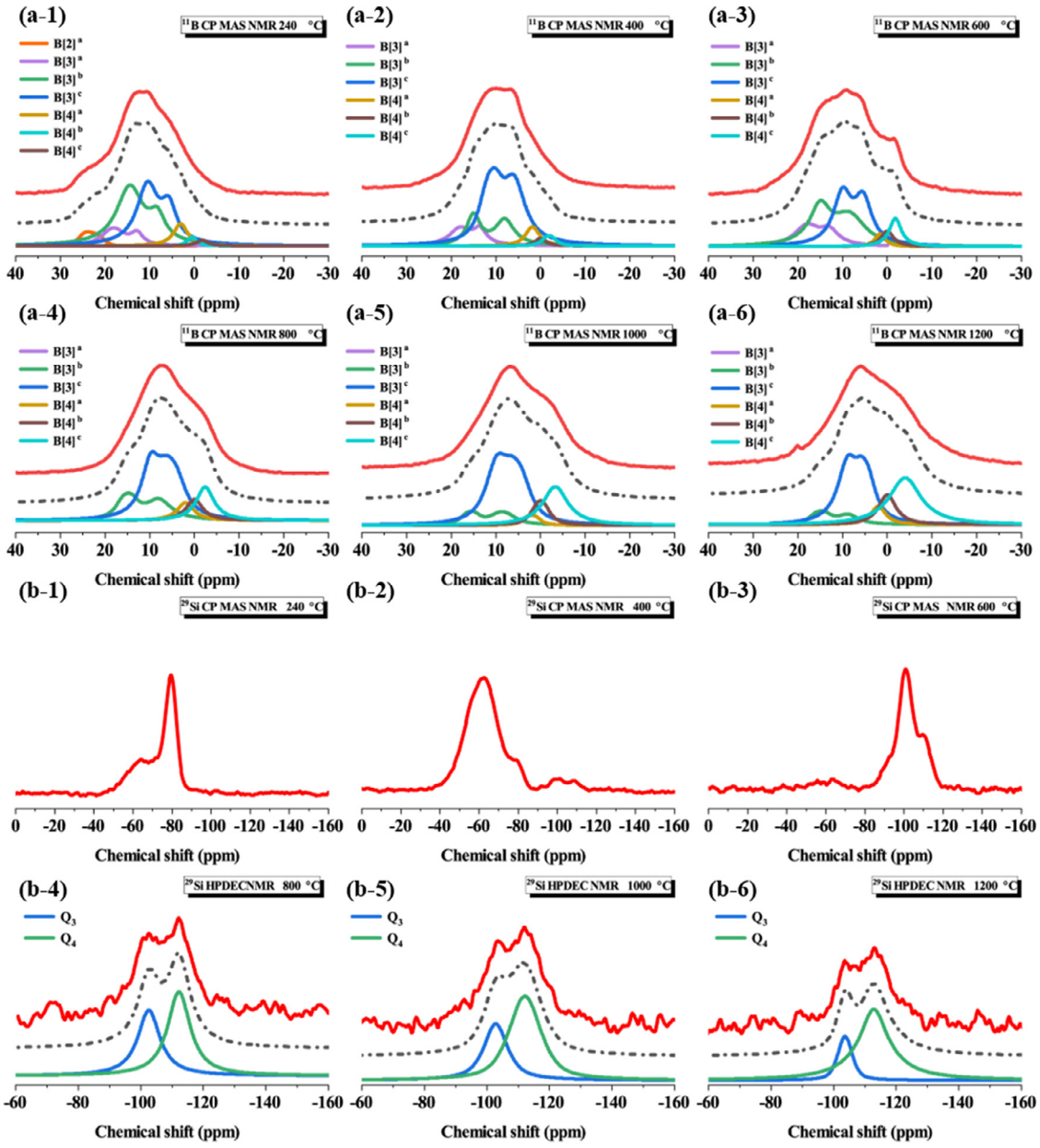

Fig. 12. Solid-state NMR spectra of the samples at different temperature during the pyrolysis stage: (a) ^{11}B solid-state NMR spectrum, and (b) ^{29}Si solid-state NMR spectrum.

tinuous oxide framework composed of B-O-B-O-Si-O-Si, endowing the hybrid resin with excellent thermal stability.

SEM was performed to investigate the morphology of the carbonization products of BSN at 800°C. As shown in Fig. 11a, the hemispherical glass layer was discovered on the surface of the carbonization matrix with a uniform distribution. The percentage coverage area and mean diameter of the hemispherical glass layer were determined using *Image J* software to be 36.8% and 130 nm, respectively. Subsequently, the elemental composition and distribution of the sample after thermal pyrolysis were determined by SEM-EDX. The SEM-EDX line scan (Fig. 11c, d, e and Fig. S3) revealed that Si, B, C, and O were uniformly distributed in the carbonization matrix and glass phase. In particular, Fig. S3 shows that the signal intensity of the C atoms in the glass phase was almost nonexistent compared with that of the carbonization matrix, which demonstrated that almost only B, Si, and O elements existed in the glass phase. In Fig. 10(a-4, b-4, and c-4), the binding energies centered at 192.9 and 193.5 eV were ascribed to B-O-B and B-O-Si bonds, respectively. Furthermore, the main components of the Si_{2p} peak at 102.1 and103.2 eV were ascribed to the Si-O-B and Si-O-Si bonds, respectively. In summary, the protective layer was confirmed to be borosilicate glass, which mainly contained SiO_2 and B_2O_3 linked by B-O-Si bonds. To explain the thermal protection mechanism of the borosilicate protective layer more clearly, the traditional PR was chosen as reference group. Fig. 10b shows that boron-silicate glass not only acted as a heat barrier to limit the heat transfer to the interior of the resin but also lowered the surface temperature of the resin by ablation [48]. The pyrolysis gas produced by the ablation of the BSN could effectively interfere with the convective heat transfer from the hyperthermia environment to the material surface. In contrast, when the glass protective layer was removed, due to the interaction of the hyperthermal environment gas, chemical and physic erosion tended to increase, which induced the formation of the rough

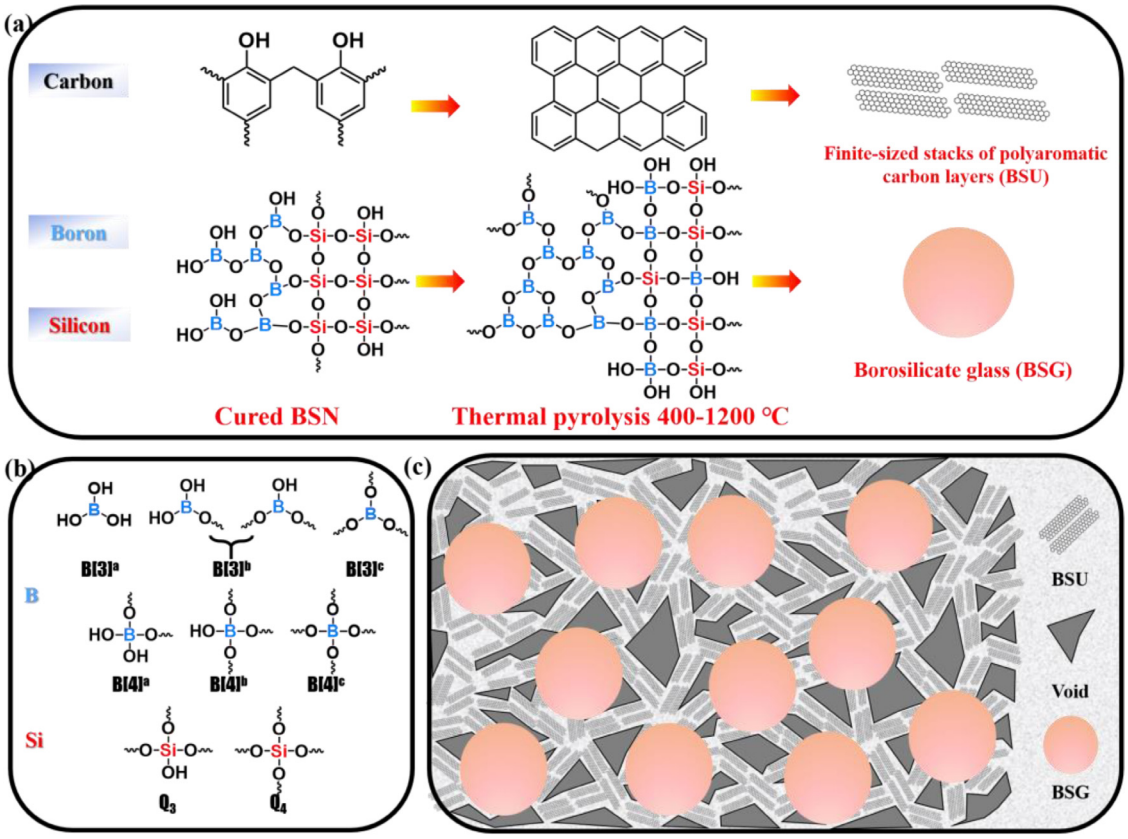

Fig. 13. Diagram of possible BSN pyrolysis process: (a) microstructural evolution of pyrolysis process of BSN100, (b) basic structural units of borosilicate glass, and (c) possible structure of pyrolysis model of BSN100.

surface of the resin, and finally led to the failure of the resin matrix.

It is known that thermally stable borosilicate glasses (e.g. DURAN and PYREX) contain at least 5% boron to achieve higher thermal stability than general silica glasses [49]. Therefore, the formation of a hemispherical borosilicate glass protective layer undoubtedly played a vital role in enhancing the excellent thermal stability of the resin. The reason the boron-silicon protective layer migrated upward and enriched the resin surface was mainly because the melting point and viscosity of borosilicate glass are relatively low [34,50]. B_2O_3 tends to combine with SiO_2 to form a low melting point eutectic mixture. Due to the reduction of melting point, the eutectic mixture is easy to overheat at lower temperatures, resulting in decreased viscosity and melt flow. Subsequently, driven by the capillary force and increasing vapor pressure [51], the eutectic mixture is forced out to enrich on the surface of the material, which acts as a glass protective layer to limit the heat flux to erode the interior of the resin matrix.

Based on the above discussions, we identified the elements and their binding characteristics on the carbonized surface, which provided a preliminary understanding of the structural evolution during the pyrolysis under heat treatment. Notably, the morphologies of the materials obtained by SEM further deepened our insight into the pyrolysis mechanism. However, both characterization techniques (SEM, and XPS) used for the materials had a similar shortcoming: the sample location, the actual location where a characteristic sample was obtained from the carbonization product, had a specific impact on the characterization result, which increased the randomness of the characterization results. The solid-state NMR techniques was used as a supplementary tool to improve the XPS and SEM results. Solid-state NMR spectroscopy serves as a valuable analysis tool to characterize chemical compositions in materials science. Due to its unique ability to assign the observed behavior to specific sites in a molecule or the macrostructure of a material, solid-state NMR techniques [38] can significantly reduce the randomness caused by the sampling process.

The ^{11}B solid-state NMR spectrum of the sample could be deconvoluted into six peaks with chemical shifts at 24 (B [2]^a), 18(B [3]^a), 15 (B [3]^b), 11 (B [3]^c), 2 (B [4]^a),0 (B [4]^b), and -2.8 ppm (B [4]^b). The presence of a chemical shift at 24 ppm was accordingly assigned to B-O-Si in the 4-HBS, and the chemical shifts at 18, 15, and 11 ppm were ascribed to the $B(OH)_3$, $B(OH)_2(OX)_1$, and $B(OX)_3$ tri-coordinated framework, respectively, where the symbol X represents adjacent boron or silicon atoms. The peaks at around 2, 0, and 2.8 ppm were assigned to the $B(OH)_2(OSi)_2$, $B(OH)_1(OSi)_3$ and $B(OSi)_4$ tetrahedral framework, respectively. As shown in Fig. 12a and Fig. S2d, the increasing intensity of the peak centered at 11 ppm (B [3]^c) indicated that the high temperature enhanced the degree of cross-linking between the B-O-B and Si-O-Si networks. Meanwhile, the emergence of peaks corresponding the tetrahedral framework further suggested that the elevated temperature drove the formation of the dual-phase of the Si-O-Si and B-O-B networks.

The solid-state ^{29}Si-NMR spectra recorded after different thermal treatments from 240°C to 1200°C are shown in Fig. 12b and Fig. S2e. Silicon atoms [41] bearing one hydroxyl group, $(Si\text{-}O)_3Si\text{-}(OH)$ (called Q_3), showed a chemical shift of 100 ppm. The Q_3 types were located mainly at the boundary of the silicate network and had high chemical reactivity. Silicon atoms without hydroxyl groups, $(Si\text{-}O)_4Si$ (called Q_4), showed a chemical shift of 109 ppm. The cleavage of the C-Si bond caused by heat treatment above 400°C indicated that a structural transformation from $RSiO_3$ to SiO_4 occurred. The area of the Q_3 and Q_4 peaks are summarized in Fig. S2e. The Q_3/Q_4 ratio is a clear indication of the degree of sil-

icon condensation. Therefore, in this work, the ratio can be used to indicate the degree of cross-linking of the Si-O-Si network. The values of the Q_3/Q_4 ratio were 0.77 (800°C), 0.54 (1000°C), and 0.24 (1200°C), respectively, indicating that high temperature greatly enhances the reactivity of Si-OH to produce a three-dimensional, more completely continuous cross-linked Si-O-Si network.

In general, the results of the above characterization provides a new perspective on the structure property relationship of BSN and clearly show that high temperatures increased the reactivity of silicon and boron units inside the resin, such as the unreacted Si-OH and B-OH located mainly at the boundary of the Si-O-Si and B-O-B networks, respectively, with high chemical reactivities [52]. The high temperature enhanced the combination of the dual-phase of the B-O-B and Si-O-Si networks to form a more extensive-scale three-dimensional continuous Si-O-Si-O-B-O-B oxide framework. Moreover, when the heat treatment temperature reached 800°C, the appearance of the B-O-C signal peak indicated the formation of covalent bonds between the Si-O-Si-O-B-O-B oxide framework and ordered polyaromatic structure during the thermal pyrolysis. The oxide framework and ordered polyaromatic structure played a vital role in enhancing the thermal stability of the resin. The addition of boron units could reduce the reaction activation energy of carbon during the graphitization and promoted the transformation of the amorphous carbon structure to the ideal graphite structure during the PR pyrolysis [13].Moreover, the terminal oxygen atom of the glassy B_2O_3 could be bonded to the chemically unstable carbon atoms of graphite, resulting in a marked reduction in the rate of oxidation of the graphite, which enhanced the degree of graphitization of the BSN resin and endowed the resin with better heat-resistance.

The characterization results for boron and silicon were consistent with the structural model proposed by Tricot et al [37]. In this model (Fig. 13b) two components coexist in the boron-silicon glass structure: a tetrahedral part and a ternary part. The tetrahedral part is based on silicate but also contains boron sites dispersed within the network, and ring and no-ring boron species together constitute the main body of the ternary part. Moreover, the tetrahedral part of the network is connected to the ternary part of the network through the B-O-Si unit. In summary, the possible structure of the pyrolysis process of the cured BSN100 is shown in Fig. 13c.

This work provides a deep understanding of the synergistic effects of boron-silicon modified PR with improved thermal stability, which can be summarized as follows:

(i) **Chemical synthesis and curing stage**: First, boron units acting as a catalyzer accelerated the hydrolysis reaction of silicon units [53]. Second, boron units serving as coupling agents participated in forming B-O-Si, B-O-C, and Si-O-C structures. These structures made the continuous Si-O-Si and B-O-B networks strongly bond to the aromatic PR skeleton, which were beneficial for improving the thermal stability of the BSN.

(ii) **Thermal pyrolysis stage:** The emergence of the B-O-Si structure indicated that the combination was determined by the chemical bonds rather than simple physical blending. The presence of the Si-O-Si network hindered the fluidity of B_2O_3 and reduced the volatilization of B_2O_3 [54–56]. Therefore, B_2O_3 could survive at higher temperatures, which indirectly improved the mass retention rate of the BSN resin. Furthermore, the B units were connected to form a B-O-B network and bind to the boundary of the Si-O-Si network by the formation of B-O-Si bonds. Such a B-O-Si bridge could effectively prevent the formation of cyclic or cage siloxane entities and lead to a larger-scale continuous Si-O-Si network [18].

4. Conclusions

In this work, an addition-curable hybrid PR containing silicon and boron were successfully obtained. By introducing VTMS with vinyl groups into the molecular structure of BSN, the hybrid resin achieved addition curing through thermal polymerization of the vinyl groups. Through the study of the curing and thermal pyrolysis mechanism of the resin, the results showed that the formation of a B-O-B-O-Si-O-Si continuous oxide framework and heat-resistant graphite structure endowed the hybrid resin with excellent thermal stability. In addition, the hemispherical boron-silicate glass protective layer was observed on the surface of the pyrolysis PR, which acted as an effective protective barrier limiting the heat flux to the resin matrix interface. As a novel hybrid PR, the BSN demonstrated its great potential in high-performance polymer composites for aerospace and aviation applications.

Declaration of Competing Interest

The authors declare that they have no known competing financial interests or personal relationships that could have appeared to influence the work reported in this paper.

CRediT authorship contribution statement

Youpei Du: Methodology, Writing – review & editing, Formal analysis, Investigation, Writing – original draft, Resources. **Yu Xia:** Resources, Writing – review & editing, Visualization, Formal analysis. **Zhenhua Luo:** Project administration, Conceptualization, Supervision, Methodology, Software, Writing – review & editing. **Wenjie Yuan:** Writing – review & editing, Visualization. **Kongli Xu:** Methodology, Software, Writing – review & editing. **Qian Wang:** Methodology, Software, Formal analysis. **Heng Zhou:** Methodology, Resources, Validation. **Ying Guo:** Methodology, Software, Validation. **Hao Li:** Methodology, Validation. **Tong Zhao:** Conceptualization, Supervision, Methodology, Software, Writing – review & editing.

Acknowledgments

The authors would like to acknowledge the financial support of National Natural Science Foundation of China (No. 51473171 & 51873215) and the Beijing Natural Science Foundation (No. 2204101). The authors also thank the following staff scientists at the center for Analysis and Testing, ICCAS for their assistance: Dr. Bo Guan, Ji-Ling Yue and Li-Yao Liu for SEM support; Ning-ning Wu and Wei Wang for ^{11}B NMR and ^{29}Si NMR support. We also thank LetPub for its linguistic assistance during the preparation of this manuscript.

Supplementary materials

Supplementary material associated with this article can be found, in the online version, at doi:10.1016/j.polymdegradstab.2021.109599.

References

[1] C.P.R. Nair, Advances in addition-cure phenolic resins, Prog. Polym. Sci. 29 (2004) 401–498.
[2] R.L. Bindu, C.P. Reghunadhan Nair, K.N. Ninan, Addition-cure phenolic resins based on propargyl ether functional novolacs: synthesis, curing and properties, Polym. Int. 50 (2001) 651–658.
[3] R.L. Bindu, C.P.R. Nair, K.N. Ninan, Phenolic resins bearing maleimide groups: synthesis and characterization, J. Polym. Sci. Part a-Polym. Chem. 38 (2000) 641–652.
[4] M. Wang, M. Yang, T. Zhao, J. Pei, Acetylene-grafted resins derived from phenolics via azo coupling reaction, Eur. Polym. J. 44 (2008) 842–848.

[5] M. Wang, L. Wei, T. Zhao, A novel condensation–addition-type phenolic resin (MPN): synthesis, characterization and evaluation as matrix of composites, Polymer 46 (2005) 9202–9210.
[6] M. Wang, L. Wei, T. Zhao, Addition-curable propargyl-containing novolac-type phenolic resin: its synthesis, characterization, cure, and thermal properties, J. Appl. Polym. Sci. 99 (2006) 1010–1017.
[7] J. Gao, Y. Liu, F. Wang, Structure and properties of boron-containing bisphenol-A formaldehyde resin, Eur. Polym. J. 37 (2001) 207–210.
[8] J. Gao, L. Xia, Y. Liu, Structure of a boron-containing bisphenol-F formaldehyde resin and kinetics of its thermal degradation, Polym. Degrad. Stab. 83 (2004) 71–77.
[9] J. Gao, Y. Liu, L. Yang, Thermal stability of boron-containing phenol formaldehyde resin, Polym. Degrad. Stab. 63 (1999) 19–22.
[10] L. Liu, B. Pan, J. Sun, X. Han, Y.A. Lei, Y. Niu, J. Luo, H. Wang, Effect of organic-mo on the wear behavior of phenolic resin composites, J. Macromol. Sci., Part B 59 (2020) 284–294.
[11] Y. Zhang, S. Shen, Y. Liu, The effect of titanium incorporation on the thermal stability of phenol-formaldehyde resin and its carbonization microstructure, Polym. Degrad. Stab. 98 (2013) 514–518.
[12] H. Li, L. Liu, Y. Zhang, K. Li, X. Shi, Y. Zhang, W. Feng, Effect of high temperature heat treatment on the ablation of SiC–ZrB2–ZrC particles modified C/C composites in two heat fluxes, J. Alloys Compd. 621 (2015) 18–25.
[13] S. Wang, X. Jing, Y. Wang, J. Si, High char yield of aryl boron-containing phenolic resins: the effect of phenylboronic acid on the thermal stability and carbonization of phenolic resins, Polym. Degrad. Stab. 99 (2014) 1–11.
[14] S. Li, Y. Han, F. Chen, Z. Luo, H. Li, T. Zhao, The effect of structure on thermal stability and anti-oxidation mechanism of silicone modified phenolic resin, Polym. Degrad. Stab. 124 (2016) 68–76.
[15] K. Haraguchi, Y. Usami, Y. Ono, The preparation and characterization of hybrid materials composed of phenolic resin and silica, J. Mater. Sci. 33 (1998) 3337–3344.
[16] K. Haraguchi, Y. Usami, K. Yamamura, S. Matsumoto, Morphological investigation of hybrid materials composed of phenolic resin and silica prepared by in situ polymerization, Polymer 39 (1998) 6243–6250.
[17] S. Li, H. Li, Z. Li, H. Zhou, Y. Guo, F. Chen, T. Zhao, Polysiloxane modified phenolic resin with co-continuous structure, Polymer 120 (2017) 217–222.
[18] C. Gervais, F. Babonneau, N. Dallabonna, G. Sorarù, Sol-gel-derived silicon-boron oxycarbide glasses containing mixed silicon oxycarbide (SiCxO4−x) and boron oxycarbide (BCyO3−y) units, J. Am. Ceram. Soc. 84 (2004) 2160–2164.
[19] S. Li, F. Chen, B. Zhang, Z. Luo, H. Li, T. Zhao, Structure and improved thermal stability of phenolic resin containing silicon and boron elements, Polym. Degrad. Stab. 133 (2016) 321–329.
[20] J. Yun, L. Chen, H. Zhao, X. Zhang, W. Ye, D. Zhu, Boric acid as a coupling agent for preparation of phenolic resin containing boron and silicon with enhanced char yield, Macromol. Rapid Commun. (2018) e1800702.
[21] C. Wang, B-x Zhang, Z. Luo, Y. Zhang, H. Zhou, Y. Guo, T. Zhao, Preparation and properties of a novel addition-curable phenolic resin containing boron element, Polym. Adv. Technol. 29 (2018) 3014–3019.
[22] C. Zha, G.R. Atkins, A.F. Masters, A spectroscopic study of an anhydrous tetraethyl orthosilicate-boric acid-ethanol system, J. Sol-Gel Sci. Technol. 13 (1998) 103–107.
[23] P. Maximiano, L. Durães, P.N. Simões, Organically-modified silica aerogels: a density functional theory study, J. Supercrit. Fluids 147 (2019) 138–148.
[24] G.D. Soraru, F. Babonneau, C. Gervais, N. Dallabona, Hybrid RSiO1.5/B2O3 gels from modified silicon alkoxides and boric acid, J. Sol-Gel Sci. Technol. 18 (2000) 11–19.
[25] A. Agarwala, T. Subramani, A. Goldbourt, D. Danovich, R. Yerushalmi, Facile monolayer formation on SiO2Surfaces via organoboron functionalities, Angew. Chem. Int. Ed. 52 (2013) 7415–7418.
[26] L. Zhang, R. Ljazouli, P. Lefaucheux, T. Tillocher, R. Dussart, Y.A. Mankelevich, J.-F. de Marneffe, S. de Gendt, M.R. Baklanov, Low damage cryogenic etching of porous organosilicate low-K materials using SF6/O2/SiF4, ECS J. Solid State Sci. Technol. 2 (2013) N131–N139.
[27] S. Li, X. Zhao, X. Liu, X. Yang, R. Yu, Y. Zhang, W. Huang, K. Deng, Cage-ladder-structure, phosphorus-containing polyhedral oligomeric silsesquinoxanes as promising reactive-type flame retardants for epoxy resin, J. Appl. Polym. Sci. 136 (2019).
[28] A. Borba, M. Almangano, A. Portugal A, R. Patricio, N. Simoes P, Methylsilsesquioxane-based aerogel systems-insights into the role of the formation of molecular clusters, J. Phys. Chem. A 120 (2016) 4079–4088.
[29] Y. Dubitsky, A. Zaopo, G. Zannoni, L. Zetta, 1H NMR study of the hydrolysis of vinyltrialkoxysilanes, Mater. Chem. Phys. 64 (2000) 45–53.
[30] D. Devapal, S. Packirisamy, J. Sreejith K, V. Ravindran P, B.K. George, Synthesis, characterization and ceramic conversion studies of borosiloxane oligomers from phenyltrialkoxysilanes, J. Inorg. Organomet. Polym Mater. 20 (2010) 666–674.
[31] A.D. Irwin, J.S. Holmgren, T.W. Zerda, J. Jonas, Spectroscopic investigations of borosiloxane bond formation in the sol-gel process, J. Non Cryst. Solids 89 (1987) 191–205.
[32] R. Di Maggio, S. Dirè, E. Callone, F. Girardi, G. Kickelbick, Si and Zr based NBBS for hybrid O/I macromolecular materials starting by preformed zirconium oxo-clusters, J. Sol-Gel Sci. Technol. 48 (2008) 168–171.
[33] H. Zhang, G. Liang, A. Gu, L. Yuan, Facile preparation of hyperbranched polysiloxane-grafted aramid fibers with simultaneously improved UV resistance, surface activity, and thermal and mechanical properties, Ind. Eng. Chem. Res. 53 (2014) 2684–2696.
[34] B. Qiu, F. Jiang, W.-D. Lu, B. Yan, W.-C. Li, Z.-C. Zhao, A.-H. Lu, Oxidative dehydrogenation of propane using layered borosilicate zeolite as the active and selective catalyst, J. Catal. 385 (2020) 176–182.
[35] A.M. Love, M.C. Cendejas, B. Thomas, W.P. McDermott, P. Uchupalanun, C. Kruszynski, S.P. Burt, T. Agbi, A.J. Rossini, I. Hermans, Synthesis and characterization of silica-supported boron oxide catalysts for the oxidative dehydrogenation of propane, J. Phys. Chem. C 123 (2019) 27000–27011.
[36] L.-S. Du, J .F. Stebbins, Site preference and Si/B mixing in mixed-alkali borosilicate glasses: a high-resolution11B and17O NMR study, ChemInform 34 (2003).
[37] G. Tricot, The structure of Pyrex(R) glass investigated by correlation NMR spectroscopy, Phys. Chem. Chem. Phys. 18 (2016) 26764–26770.
[38] L.-S. Du, J.F. Stebbins, Solid-state NMR study of metastable immiscibility in alkali borosilicate glasses, J. Non Cryst. Solids 315 (2003) 239–255.
[39] B. Liang, J. Wang, J. Hu, C. Li, R. Li, Y. Liu, K. Zeng, G. Yang, TG-MS-FTIR study on pyrolysis behavior of phthalonitrile resin, Polym. Degrad. Stab. (2019) 169.
[40] S. Wang, Y. Wang, C. Bian, Y. Zhong, X. Jing, The thermal stability and pyrolysis mechanism of boron-containing phenolic resins: the effect of phenyl borates on the char formation, Appl. Surf. Sci. 331 (2015) 519–529.
[41] P. Legrand A, H. Hommel, B. d'Espinose de la Caillerie J, On the silica edge: an NMR point of view, ChemInform (2006) 37.
[42] Q. Ren, L. He, S. Hu, H. Li, S. Li, Z. Deng, G. Song, S. Su, Y. Wang, J. Xiang, Formation of highly graphitic char derived from phenolic resin carbonization by Ni-Zn-B alloy, Environ. Sci. Pollut. Res. Int. (2020).
[43] F. Badaczewski, M.O. Loeh, T. Pfaff, S. Dobrotka, D. Wallacher, D. Clemens, J. Metz, M. Smarsly B, Peering into the structural evolution of glass-like carbons derived from phenolic resin by combining small-angle neutron scattering with an advanced evaluation method for wide-angle X-ray scattering, Carbon 141 (2019) 169–181.
[44] Z.L. Yu, B. Qin, Z.Y. Ma, J. Huang, S.C. Li, H.Y. Zhao, H. Li, Y.B. Zhu, H.A. Wu, S .H. Yu, Superelastic hard carbon nanofiber aerogels, Adv. Mater. (2019) e1900651.
[45] T. Semoto, Y. Tsuji, H. Tanaka, K. Yoshizawa, Role of edge oxygen atoms on the adhesive interaction between carbon fiber and epoxy resin, J. Phys. Chem. C 117 (2013) 24830–24835.
[46] D.W. McKee, C.L. Spiro, E.J. Lamby, The effects of boron additives on the oxidation behavior of carbons, Carbon 22 (1984) 507–511.
[47] Y.-S. Wei, W.-Y. Liu, H.-M. Wu, K.-S. Chen, V. Cech, Characteristics of SiOx–containing hard film prepared by low temperature plasma enhanced chemical vapor deposition using hexamethyldisilazane or vinyltrimethylsilane and post oxygen plasma treatment, Mater. Chem. Phys. 189 (2017) 183–190.
[48] M. Natali, M. Kenny J, L. Torre, Science and technology of polymeric ablative materials for thermal protection systems and propulsion devices: a review, Prog. Mater Sci. 84 (2016) 192–275.
[49] E.-B. Cho, M. Mandal, M. Jaroniec, Periodic mesoporous benzene−silicas prepared using boric acid as catalyst, Chem. Mater. 23 (2011) 1971–1976.
[50] W. Wang, S. Dai, L. Zhou, J. Zhang, W. Tian, J. Xu, Viscosity and structure of MgO–SiO2-based slag melt with varying B2O3 content, Ceram. Int. 46 (2020) 3631–3636.
[51] D. Zhang, P. Hu, S. Dong, X. Liu, C. Wang, Z. Zhang, X. Zhang, Oxidation behavior and ablation mechanism of Cf/ZrB2-SiC composite fabricated by vibration-assisted slurry impregnation combined with low-temperature hot pressing, Corros. Sci. (2019) 161.
[52] R. Simonutti, A. Comotti, S. Bracco, A. Simonelli, P. Sozzani, Nanoporous silica grown in organic media: absorption and NMR characterization, Chem. Mater. 14 (2002) 3377–3381.
[53] S. Ding, N. Liu, X. Li, L. Peng, X. Guo, W. Ding, Silica nanotubes and their assembly assisted by boric acid to hierachical mesostructures, Langmuir 26 (2010) 4572–4575.
[54] S. Fan, X. Ma, B. Ji, Z. Li, Z. Xie, J. Deng, L. Zhang, L. Cheng, Oxidation resistance and thermal shock properties of self-healing SiCN/borosilicate glass-B4C-Al2O3 coatings for C/C aircraft brake materials, Ceram. Int. 45 (2019) 550–557.
[55] X. Zhao, Y. Wang, L. Duan, L. Luo, Y. Lu, Improved ablation resistance of C/SiC-ZrB2 composites via polymer precursor impregnation and pyrolysis, Ceram. Int. 43 (2017) 12480–12489.
[56] A.S. Zelenev, J.M. Fu, B.A. Keiser, Establishing the difference between colloidal borosilicate and boron-modified colloidal silica via chelation of boron with catechol and dl-tartaric acid, Polyhedron 26 (2007) 4941–4944.